Journal of Alloys and Compounds, Volume 735, 2018, Pages 861-869
DOI:10.1016/j.jallcom.2017.11.104

Enhanced thermoelectric performance of Cs doped BiCuSeO prepared through eco-friendly flux synthesis

Abdenour Achour[a], Kan Chen[b], Mike .J. Reece[b], and Zhaorong Huang[a]

[a]Surface Engineering and Nanotechnology Institute, Cranfield University, Bedfordshire, MK43 0AL, UK

[b]Department of Materials, Queen Mary University of London, Mile End Road, London E1 4NS, UK

Corresponding author: A.Achour@cranfield.ac.uk

Abstract – The synthesis of BiCuSeO oxyselenides by a flux method in air has been investigated. A maximum power factor of 230 $\mu Wm^{-1}K^{-2}$ and a very low thermal conductivity of 0.42 $Wm^{-1}K^{-1}$ were obtained, leading to a high ZT value of 0.37 at 680 K for pristine BiCuSeO. With Cs doping, a large enhancement in electrical conductivity coupled with a moderate decrease in Seebeck coefficient lead to a power factor of 340 $\mu Wm^{-1}K^{-2}$ at 680 K. In addition, Cs doping reduced the thermal conductivity further to 0.35 $Wm^{-1}K^{-1}$ at 680 K. The combination of higher power factor and reduced thermal conductivity results in a high ZT value of 0.66 at 680 K for $Bi_{0.995}Cs_{0.005}CuSeO$.

Keywords

BiCuSeO; Thermoelectric materials; Cs doping; Flux synthesis; Thermal conductivity

Published by Elsevier. This is the Author Accepted Manuscript issued with: Creative Commons Attribution Non-Commercial No Derivatives License (CC:BY:NC:ND 4.0). The final published version (version of record) is available online at DOI:10.1016/j.jallcom.2017.11.104. Please refer to any applicable publisher terms of use.

1. Introduction

Nearly 70 % of the world's useful energy is lost as waste heat. Among the viable technologies for energy recovery, thermoelectrics (TE) can capture and transform waste heat directly into electric power [1–3]. This is based on the Seebeck effect, where an electromotive force develops when a material is exposed to a temperature gradient. Moreover, these TE devices do not have moving parts, such as in a compressor, which make them free of noise and vibration. The existing TE technologies can convert less than 10% of heat energy into electricity [3,4]. This conversion efficiency depends on a dimensionless figure of merit ZT, which only depends on the intrinsic properties of the materials, defined as [5]:

$$ZT = S^2\sigma\, T/\kappa \quad (1)$$

where σ is the electrical conductivity, S is the Seebeck coefficient, κ is the thermal conductivity and T is the absolute temperature. Despite the high ZT values of some metallic alloys, their thermal instability, high-cost and toxic constituent elements, make these materials difficult to use for large scale application and commercialisation [6]. To overcome these disadvantages, several families of oxide-based materials have been investigated as promising TE materials, these include: perovskite-like compounds such as $SrTiO_3$ [7,8], $CaMnO_3$ [9]; layered compounds such as $Ca_3Co_4O_9$ [10] and $NaCoO_2$ [11], and simple oxides like ZnO [12] and In_2O_3 [13].

Recently, a promising middle temperature range TE system based on the oxyselenides BiCuSeO (BCSO) has been reported. BCSO materials have high ZT values due to its intrinsically low thermal conductivity and relatively large Seebeck coefficient. As a p-type TE, the Seebeck coefficient for BCSO was found to be over 300 μV/K at about 600 K [14-19], as compared to less than 200 μV/K for other p-type TE materials such as $Na_{0.85}CoO_2$ and $Ca_3Co_4O_9$ at 673K [10-11]. Moreover, its ZT value has been improved by optimizing electrical conductivity through the partial substitution of Bi^{3+} with bivalent elements (ZT values for Mg, Sr, Ca and Ba were 0.67, 0.76, 0.9 and 1.1 respectively at 923 K) and a monovalent element (ZT value for Na was 0.97 at 873 K) [14–19]. More recently, a high ZT value of 1.4 for Ba-doped BCSO via grain-texturing and modulating doping has been obtained [20,21]. Furthermore,

the ZT has been boosted to the maximum value of 1.5 at 873 K via a dual-doping approach [22]. However, little attention has been paid to new methods of synthesis.

In this paper, a B_2O_3 flux method to synthesise BCSO thermoelectric compounds in air is reported. Boron oxide serves as a liquid-seal on the top of the raw materials during the reaction process. This can inhibit stoichiometric balance modification between Bi, Se, Cu and O elements. Moreover, there is no need to maintain a vacuum or use a sealed evacuated quartz tube, which makes it easier for scaling up for batch production. Furthermore, the microstructure, thermal and chemical stability and electro-thermal properties of BCSO have been investigated and compared to previously reported methods. It was also demonstrated that Cs doping improves the ZT by enhancing the electrical conductivity and reducing the thermal conductivity.

2. Experimental

A series of polycrystalline $Bi_{1-x}Cs_xCuSeO$ (x = 0 – 0.025) powders were synthesized using a facile one-step boron oxide flux method in air. Stoichiometric amounts of Bi_2O_3 (99.9%, Alfa-Aesar), Bi (99.999%, Alfa-Aesar), Cu (99.99%, Alfa-Aesar), Se (99.999%, Alfa-Aesar), and Cs_2CO_3 (99.99%, Alfa-Aesar) powders were weighted, homogeneously ground in an agate mortar, and then transferred into an alumina crucible. The later was covered with B_2O_3 (99%, Alfa-Aesar) powder and compacted. The crucible was placed into a chamber furnace, heated at 873 K for 10 hours and finally cooled down to room temperature. After smashing the alumina crucible, the obtained product and the B_2O_3 flux were easily separated from each other. During the flux synthesise, the boron oxide melts and serves as a liquid-seal on the top of the crucible. The obtained product of each sample was then ground to a fine powder and sintered using a spark plasma sintering (SPS) furnace (SPS/FAST Model FCT, HP, D 25-SD) under an axial compressive stress of 50 MPa at 923 K for 10 min, to form dense pellets of Φ 20 mm x 3 mm. The phase structure and purity were investigated using X-ray diffraction (XRD, Siemens D5000). The morphology of samples was obtained using a scanning electron microscope (SEM, FEI XL30 SFEG). The SPSed samples were cut into bars with dimensions 3.5 x 3 x 13 mm^3 for the simultaneous measurements of the Seebeck coefficient and the electrical conductivity along the perpendicular direction to the SPS axial pressure using a Linseis LSR-3 system under a helium atmosphere. Of note, these bar samples were cut along the transverse

direction to SPS axial pressure of the disc-shaped samples. The thermal diffusivity (α) was measured along the SPS axial pressure direction, by using a Netzsch LFA-457 laser flash system under continuously flowing argon. The total thermal conductivity (κ) was calculated using the equation $\kappa = \alpha C_p \rho$, where ρ is the mass density measured by the Archimedes method, while C_p is the specific heat. The thermogravimetry (TG) and the differential scanning calorimetry (DSC) of the bulk samples were analysed simultaneously by thermal analysis (Setaram Setsys Evolution 16/18) up to ~ 1010 K with a heating rate of 10 K min^{-1}, and a flow rate of 20 mL min^{-1} under argon or air; α-Al_2O_3 was used as a reference material.

3. Results and Discussion

3.1 Fabrication Process and Structure Analysis

The fabrication procedures used to prepare $Bi_{1-x}Cs_xCuSeO$ (x = 0 – 0.025) samples are presented in **Fig. 1**. As shown in **Fig. 1(a)**, the starting materials were loaded into a crucible, compacted and covered with boron oxide powder. Despite the low melting points of Se (T_m ~ 490 K, ρ ~ 4.81 g/cm^3) and Bi (T_m ~ 544 K, ρ ~ 9.78 g/cm^3) compared to that of B_2O_3 (T_m ~ 723 K, ρ ~ 2.46 g/cm^3), the boron oxide did not infiltrate into the BCSO, at least at the end of the synthesis (**Fig. 1(b))**. This suggested that the protective B_2O_3 liquid-seal was formed at the top of the BCSO, due to its smaller density than the other raw materials. The separation of the produced BCSO and the B_2O_3 was very simple. Hence, the obtained material was uniform and rigid as shown in **Fig. 1(c)**. The obtained product was ground to a powder and SPS sintered to produce dense pellets for further structural and TE properties characterizations (**Fig. 1(d)**).

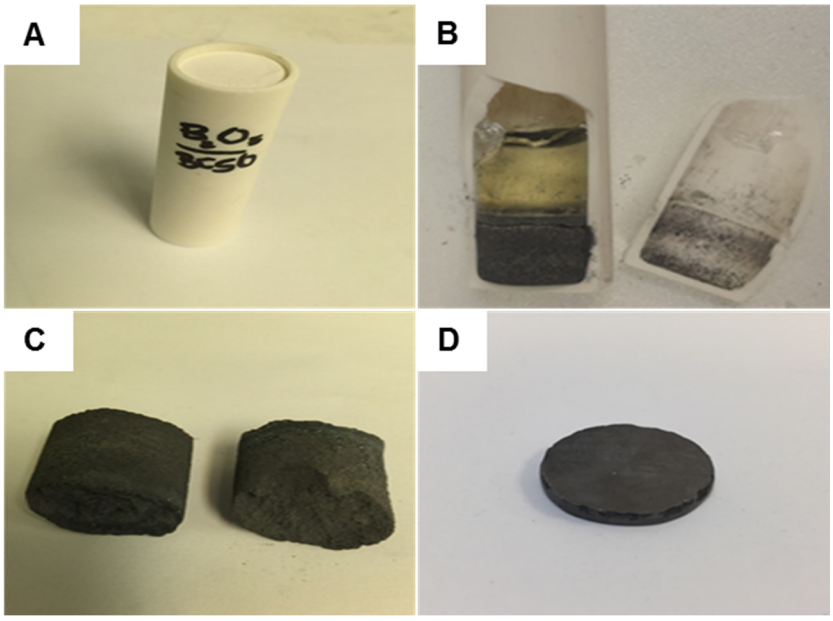

Fig. 1. Fabrication process of BCSO samples: (a) alumina crucible filled with raw chemicals; (b) broken alumina crucible after flux synthesis; (c) as – synthesized products after the removal of B_2O_3; (d) a SPSed pellet.

Fig. 2(a) shows the different positions and a cross-section of a BCSO sample where X-ray diffractions were performed. The top (Z1) and middle (Z2) positions were about 1 mm, and 5 mm from the glassy B_2O_3 respectively. The position Z3 was at the bottom side of the produced BCSO. The cross section was cut through the middle of the same sample. **Fig. 2(b)** shows XRD patterns for these three positions and the cross section. The BCSO delineated a single-phased ZrSiCuAs-type tetragonal crystal structure (space group, P4/nmm), except that a minor amount of Bi_2O_3 impurity was detected at the three positions Z1-Z3. The cross-section of the sample did not show a peak of Bi_2O_3. This suggested that reaction to form the BCSO crystal phase was complete at the center of the crucible at least, and a incomplete reaction occurred at the outmost part of the sample only. The lack of boron oxide peaksT indicated that either the diffusion between boron oxide and raw materials did not occur, or only happened at the top of the sample which had already been removed.

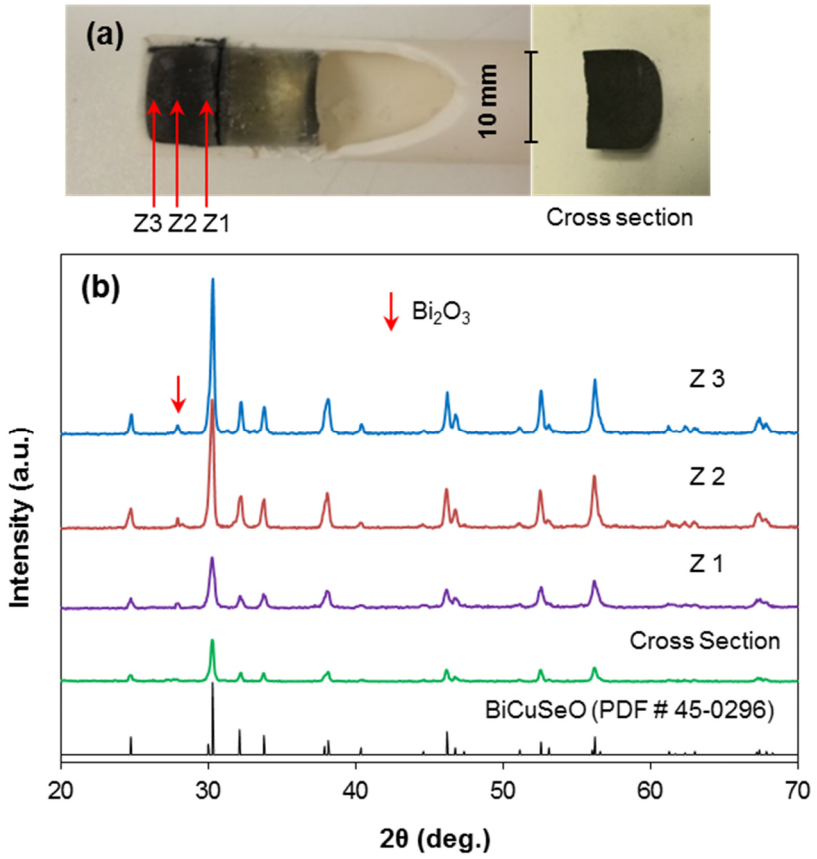

Fig. 2. (a) Photograph; (b) XRD patterns for different positions Z1, Z2, Z3, and a cross section of the as-synthesised undoped BCSO.

The product as synthesized was highly rigid and could be easily ground. Shown in **Fig. 3** are XRD patterns of the product after grinding and the following SPSed pellets. It can be seen that no Bi_2O_3 peak could be observed and all the XRD peaks were indexed to the BCSO (PDF#45-0296). This indicated that the Bi_2O_3 peak observed in Fig. 2 existed at only the outmost part of the sample, the vast majority of the powders were single phased ZrSiCuAs-type crystal structure. After grinding of the as-prepared sample, the tiny amount of Bi_2O_3 as compared to the total amount of BCSO made the Bi_2O_3 concentration beyond the detection limit of the XRD in the mixed and grinded sample.

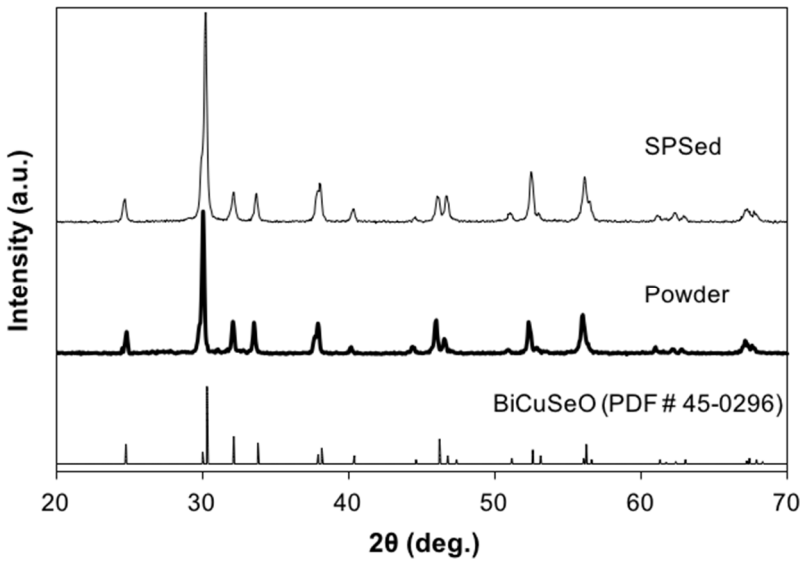

Fig. 3. XRD patterns of pure BCSO powder and SPSed pellet.

Fig. 4(a) shows XRD patterns of the $Bi_{1-x}Cs_xCuSeO$ after SPS treatment. All samples with different doping concentrations (x = 0 – 0.015) demonstrated a pure phase of tetragonal crystal structure as indexed by PDF#45-0296. However, for the 2.5 mol% Cs-doped sample, a minor Bi_2O_3 phase was observed. Of course, a tiny amount of Bi_2O_3 phase could have existed in the lower doped samples as well, but it could not be detected using XRD analysis due to the limited detectability of the technique. Recently, it was reported that elemental doping at Bi site generally leads to a Bi_2O_3 impurity, which can affect the phase purity and thermoelectric performance of the materials by affecting the carrier mobility and thereby lowering the electrical conductivity [23,24]. **Fig. 4(b)** shows the magnified XRD pattern which shows clearly a shift of the peak position between 29.5^o and 30.5^o, and also for the peaks in the range from 52^o to 57^o with the increasing doping concentration.

The lattice parameters for these samples were obtained using the XRD data. As can be observed in **Fig. 4(c)**, the lattice constants increased almost linearly with doping concentration and this can be explained by the Cs introduced into the BCSO. However, for 2.5% Cs doped the lattice parameters decreased, which was consistent with the presence of an amount of secondary phase. This suggests that the solubility limit was reached for Cs content between 1.5% and 2.5%.

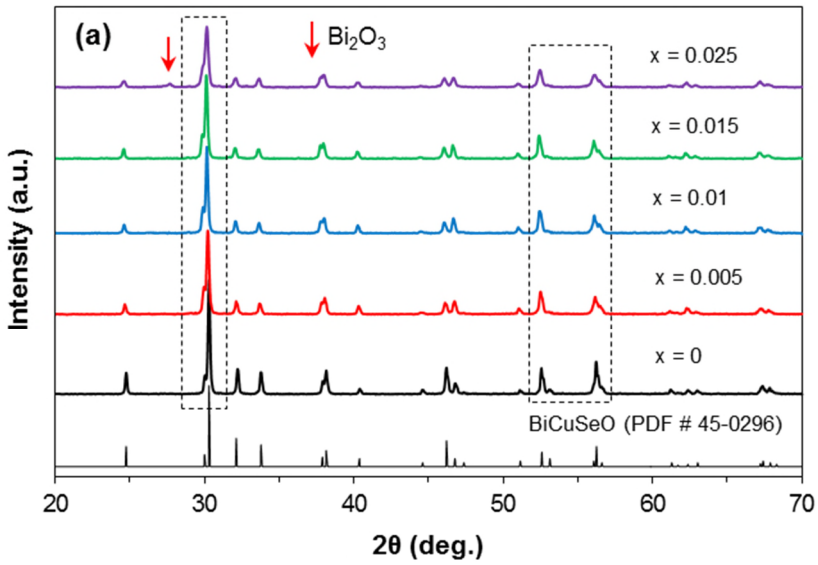
(a)
Bi2O3
x = 0.025
x = 0.015
x = 0.01
x = 0.005
x = 0
BiCuSeO (PDF # 45-0296)
Intensity (a.u.)
20
30
40
50
60
70
2θ (deg.)

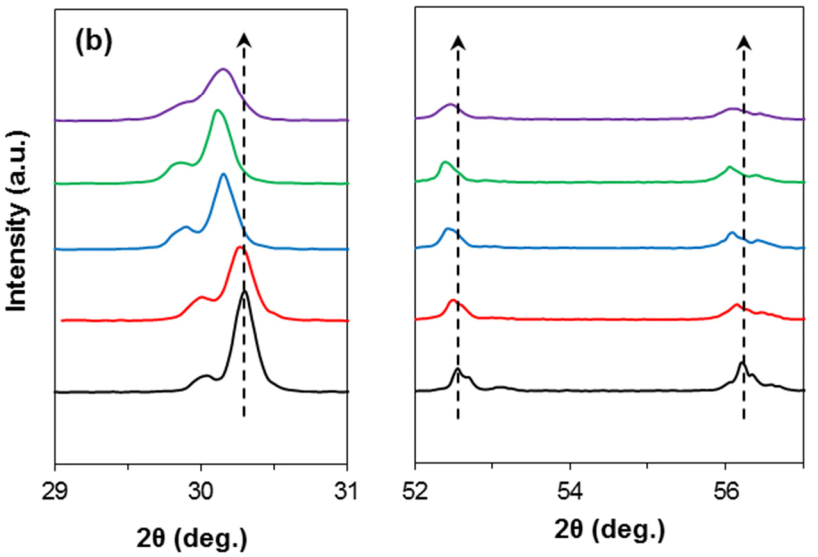
(b)
Intensity (a.u.)
29
30
31
2θ (deg.)
52
54
56
2θ (deg.)

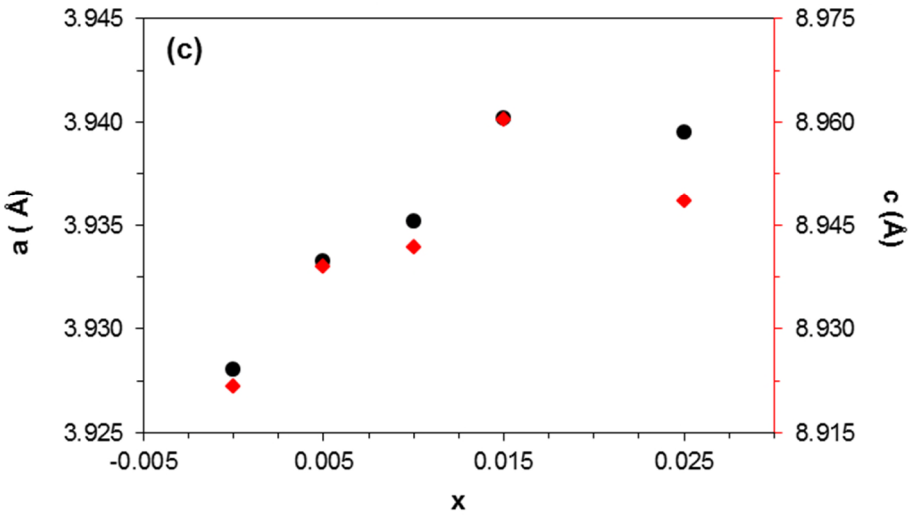
(c)
3.945
3.940
3.935
3.930
3.925
a (Å)
8.975
8.960
8.945
8.930
8.915
c (Å)
-0.005
0.005
0.015
0.025
x

Fig. 4. (a) XRD patterns; (b) enlarged peaks for sections of (a); (c) lattice parameters of $Bi_{1-x}Cs_xCuSeO$.

The expansion of the unit cell along the c axis might be related to the much larger ionic radius of Cs^+ (1.67 Å) as compared to that of Bi^{3+} (1.03 Å) and Cu^+ (0.77 Å). The pronounced effect to the lattice parameters can also be attributed to weakening of the coulombic forces between the layers due to the aliovalent doping, which modifies the electronic charge of each layer.

3.2 Morphology and Microstructure Analysis of the SPSed samples

The morphology and microstructure of the freshly broken cross section of SPSed samples of the pristine BiCuSeO and Cs-doped samples are shown in **Fig. 5**. From the SEM image, a highly dense morphology can be observed. The bulk density as measured by the Archimedes method of the sintered materials reached 97% of the theoretical value (**Table 1**). As shown in **Fig. 5(a)**, a larger grain size of 2-6 μm was observed, which was larger than 1-2 μm for those synthesized by using self-propagating high-temperature method (SHS) [25] and much larger than 400-800 nm obtained using solid-state reaction route (SSR) [19]. SEM images showed that the grain size was progressively reduced with the increasing Cs doping. Reduced grain size generated a larger number of grain boundaries, which may reduce the thermal conductivity via phonon scattering. Furthermore, the grain size of the doped sample was much smaller than that of the pure BCSO (**Fig. 5(a)**). This indicates that the grain size reduction might be due to the repressed growth with Cs doping.

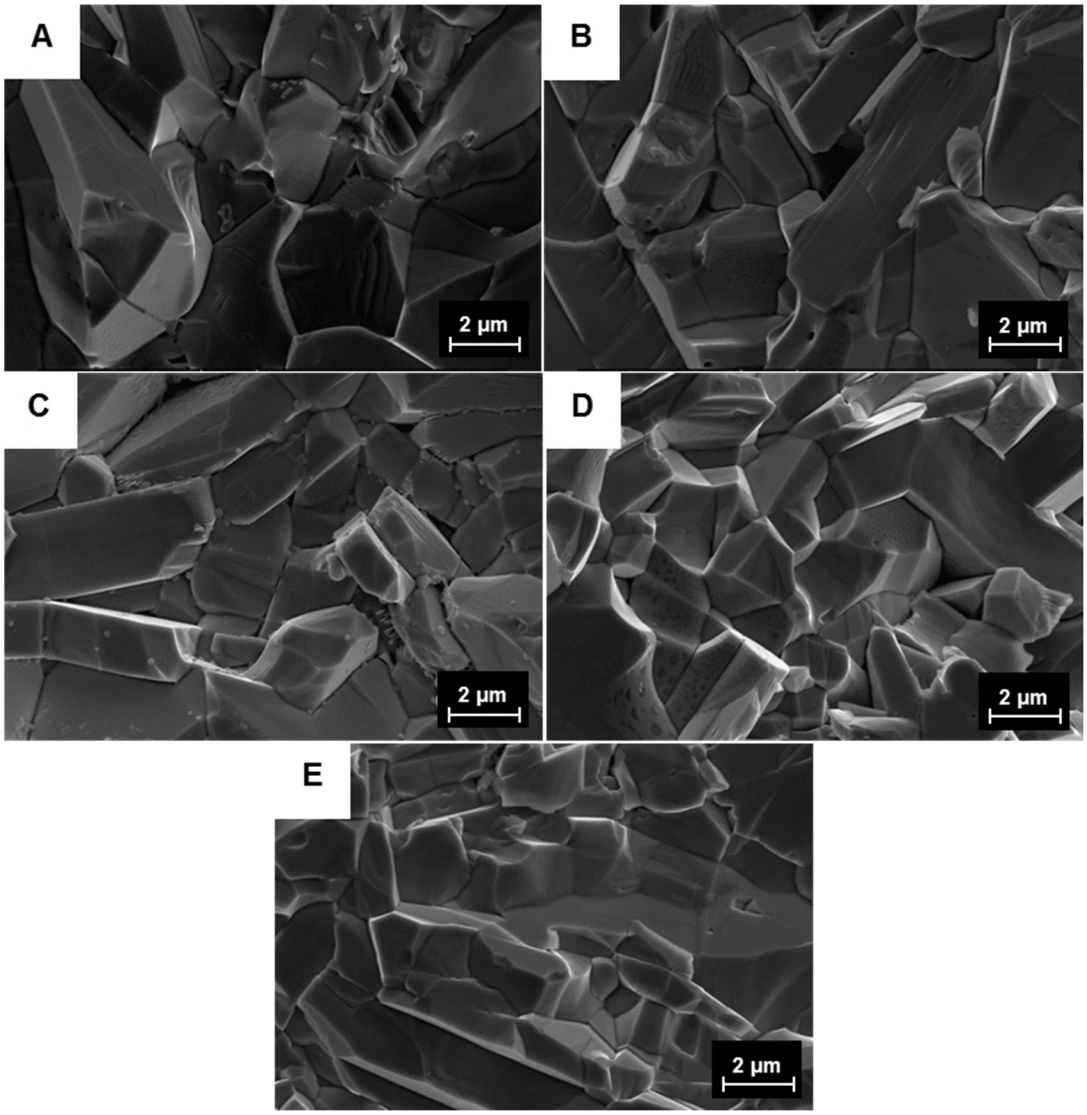

Fig. 5. SEM cross section images of $Bi_{1-x}Cs_xCuSeO$ (x = 0 – 0.025) synthesized by flux – SPSed: (a) x = 0; (b) x = 0.005; (c) x = 0.01; (d) x = 0.015; (e) x = 0.025.

3.3 Thermal and Chemical Stability

Thermoelectric generator devices are usually subjected to large thermal stresses and strains for a long period of time. Therefore, it is necessary to study their thermal and chemical stability. **Fig. 6** shows the differential scanning calorimetry (DSC) and thermogravimetric analysis (TGA) curves of SPSed $Bi_{1-x}Cs_xCuSeO$ under either flowing argon or air. Under argon flow, below a caesium content of x = 0.005, no weight change or no obvious endothermic or exothermic peaks appeared at temperatures up to 923 K, which indicated the stability of these materials (**Fig. 6(a)**). However, a clear endothermic peak was observed around 1000K and accompanied by ~ 1.5 %

weight loss in the TGA curves (**Fig. 6(b)**). The undoped BCSO result is similar to the one reported by Barreteau and Li who observed DSC peaks at 1023 K [26,27].

At and above a caesium content of x = 0.01, a clear change of the slop of the curve was observed from 680 K where decomposing starts under argon and air conditions (**Fig. 6(a)**). Upon further heating, two endothermic peaks were observed, a small peak around 750 – 850 K and a broader peak between 900 – 1010 K, and the accompanied total weights loss were about 2.3 % (**Fig. 6(b)**). It is noteworthy that the stability of the phase was reduced and the onset temperature of the broader peak decreased with increasing caesium content. Although the Selenium element can be partially volatilized at atmospheric oxidizing condition at temperatures as low as 473 K [27–29], the BCSO samples exhibited good resistivity against volatility.

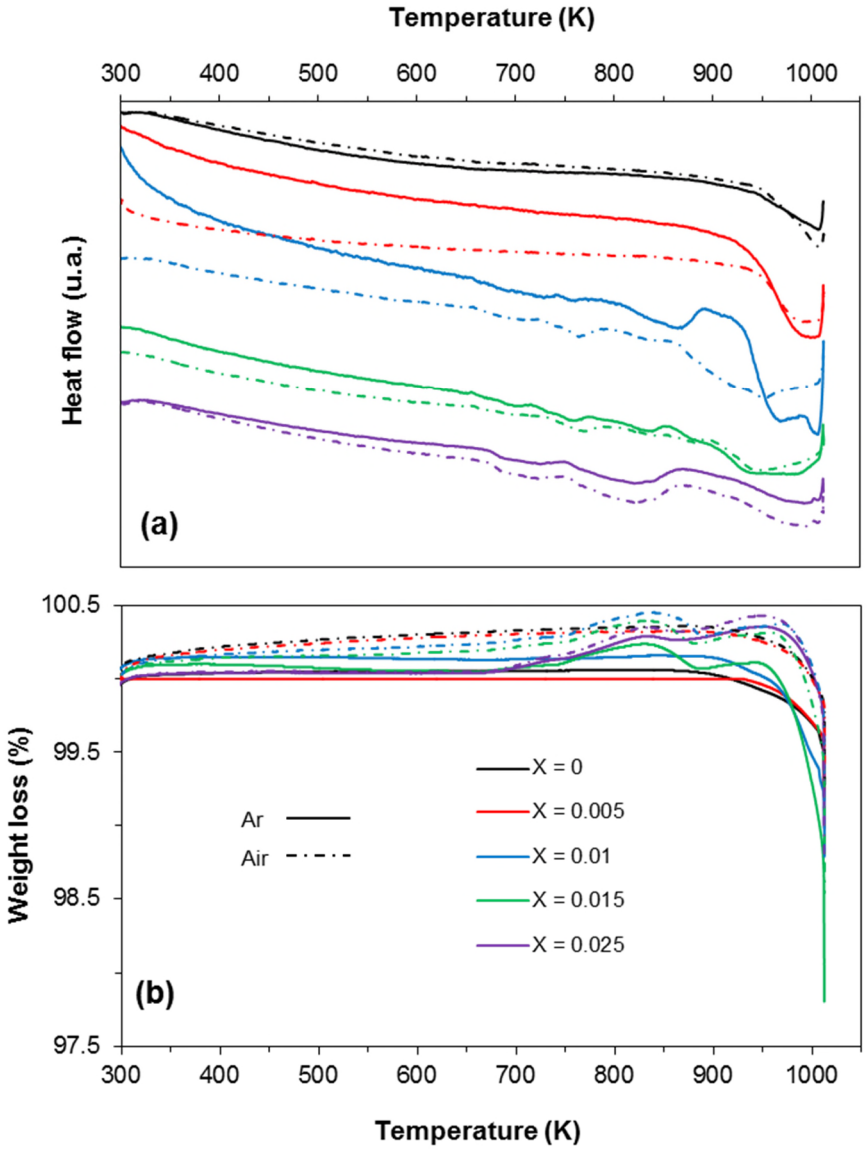

Fig. 6. (a) Differential scanning calorimetry; and (b) thermogravimetric analysis of $Bi_{1-x}Cs_xCuSeO$ (x = 0 – 0.025) samples under flowing argon and air.

Mass gain was observed in all samples under air flow from 300 to ~ 960 K and then a significant decrease of mass above 960 K. This indicates oxidation of the BCSO happened when it was heated in air. TGA curves show a maximum of 0.4 % gain in weight at 850 K for $Bi_{0.99}Cs_{0.01}CuSeO$. However, no obvious exothermic peak (reflecting the formation of a secondary phase) on DSC was observed. Surprisely, mass gaining was observed from 700 K to 950 K for 1.5% and 2.5% Cs doped samples under pure argon flow, suggesting a gas leakage of the system at temperatures above 700 K at least.

Fig. 7 displays bar-samples of Cs doped BCSO (0.5 and 1%) after thermoelectric property measurement. The image discloses an obvious change at the surface of the sample of 1% (**Fig. 7(b)**) Cs and above, but not for the 0.5% Cs or non-doped BCSO. This confirms the results in **Fig. 6(a) that** changes of the slope of the DSC curves for 1% Cs doping and above but not for the 0.5% Cs or non-doped.

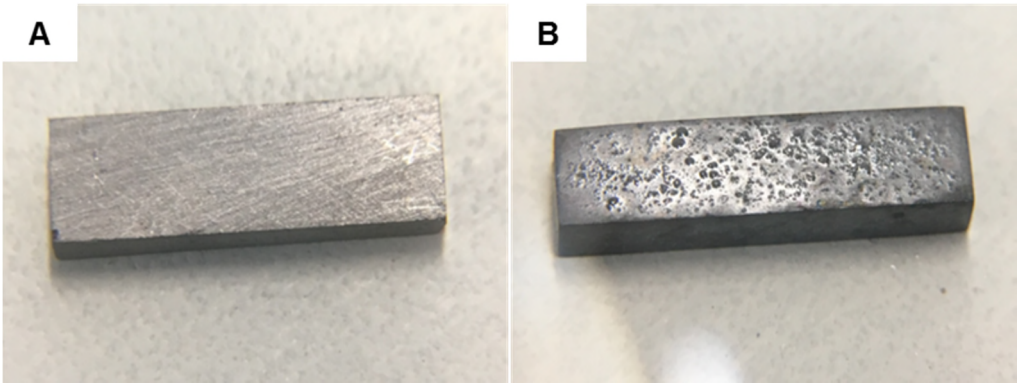

Fig. 7. Bar-sample of Cs Doped BCSO after TE measurements: (a) 0.5%; (b) 1%.

Moreover, compositional analysis was carried out by EDS (**Fig. 8**). The quantitative data of the $Bi_{0.99}Cs_{0.01}CuSeO$ sample confirmed there were two coexisting areas, each had different elemental composition (**Table 2**): (1) the dark area, which had a high Cs concentration of more than 80 Wt. %; (**Fig. 8(b)**), and (2) the bright or white area, where Cs content was close to the stoichiometric concentration (**Fig. 8(c)**). These results conform to the previous conclusion that that the highly-doped $Bi_{1-x}Cs_xCuSeO$ ($x \geq 0.01$) materials were not stable when heated (during the TE property measurement) in air, and suggest the dark aggregates in Fig. 7(b) were Caesium oxide.

Table 1. Elemental quantification results showing the typical composition found at the $Bi_{0.99}Cs_{0.01}CuSeO$ sample.

Elements	Wt. % - Dark area	Wt. % - Clear area
Cu	0.91	21.01
Se	11.79	21.57
Cs	85.01	3.55
Bi	2.28	53.87
Totals	100	100

In summary these results suggest that the undoped BCSO and up to 0.5% Cs-doped BCSO materials were stable under argon atmosphere below 923 K. Moreover, it appears that Se volatilization was not an issue for the use of BCSO based materials as thermoelectric modules under inert atmosphere. This agrees with the report that no significant weight loss was observed for SPSed pure BCSO for several days at 923 K [20]. Using a powder with high specific area of 0.255 m^2 g^{-1}, the total weight loss less than 1 % was observed for powders after 3-week. This meant even if the whole surface of a BCSO cube is exposed to a high temperature of 923 K, it would take more than one year to observe 1% weight loss [26].

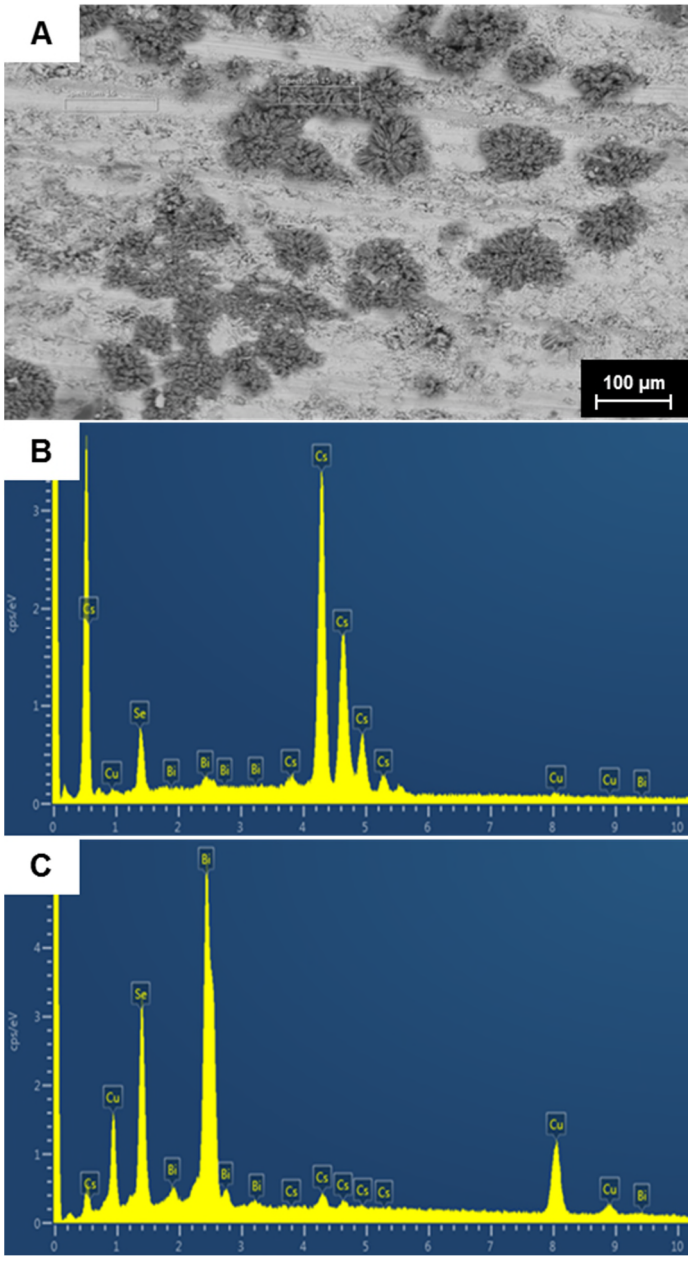

Fig. 8. SEM image, EDS spectrums showing the typical composition found at the $Bi_{0.99}Cs_{0.01}CuSeO$ sample.

3.4 Thermoelectric Properties Characterisation

3.4.1 Pristine BiCuSeO

In order to compare the thermoelectric properties of the flux route with previously reported methods, the temperature dependence of thermoelectric properties of the undoped BCSO were measured over the temperature range 315 – 764 K. These

values were compared with undoped BCSOs prepared by SHS and SSR methods [19,25,30] and displayed in **Fig. 9** and **Fig. 10**. As seen in **Fig. 9(a)**, the electrical conductivity of the sample synthesized using the flux method (18.8 S/cm at 764 K) was higher than that SSR route (~ 10 S/cm at 775 K) but lower than that of SHS synthesis (~ 45.4 S/cm at 775 K).

The comparison of Seebeck coefficient among these methods was shown in **Fig. 9(b)**. A similar trend of the Seebeck coefficient was observed for the flux and SHS methods, but different to that of the materials prepared using SSR method. At room temperature, the highest Seebeck coefficient was observed for the flux method at 516 μV/K, and then decreased with the increase of temperature (328 μV/K at 764 K). In **Fig. 9(c)**, a power factor value of ~ 230 μW m^{-1} K^{-2} at 665 K was obtained for the materials prepared using the flux method, which was higher than that of SSR method (~ 174 μW m^{-1} K^{-2} at 775 K) but lower than that of SHS (~ 375 μW m^{-1} K^{-2} at 775 K). The large power factor can be attributed to the high electrical conductivity and the high Seebeck coefficient.

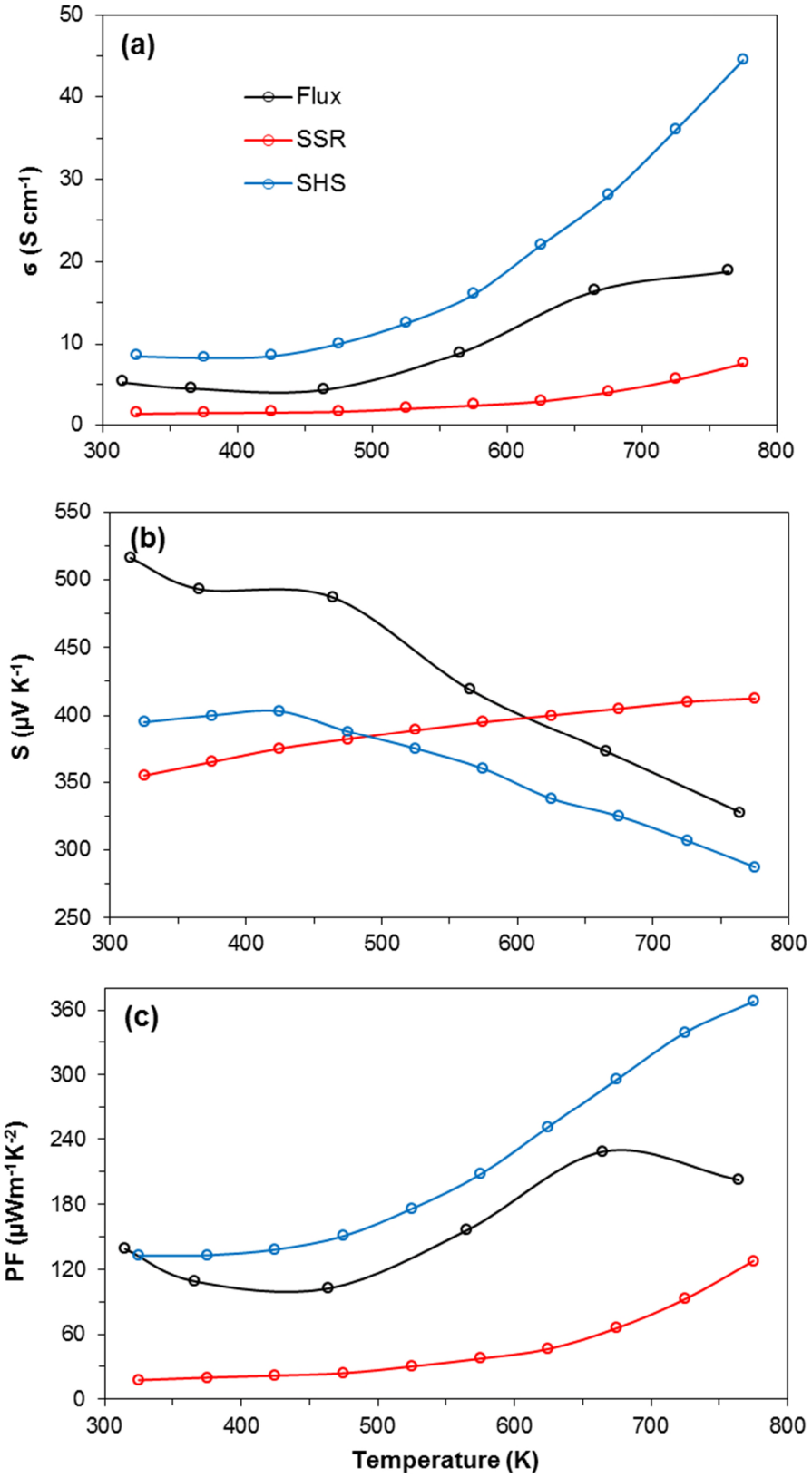

Fig. 9. Temperature dependence of thermoelectric properties for the BCSO synthesized by SSR, SHS and the flux methods: (a) electrical conductivity; (b) Seebeck coefficient; (c) power factor.

Fig. 10(a) shows the thermal conductivity (κ) as a function of temperature for SPSed BCSO synthesized by the flux method, which decreased continuously with temperature. Compared to the SHS and SSR methods, the flux method showed lowest thermal conductivity in the whole temperature range, ~ 0.84 $Wm^{-1}K^{-1}$ at 315 K and ~ 0.42 $Wm^{-1}K^{-1}$ at 765 K. These values are lower than most thermoelectric materials. These relatively low thermal conductivity values were attributed by the low lattice contribution and may originated from the weak bonding between the layers and the low Young's modulus [31,32].

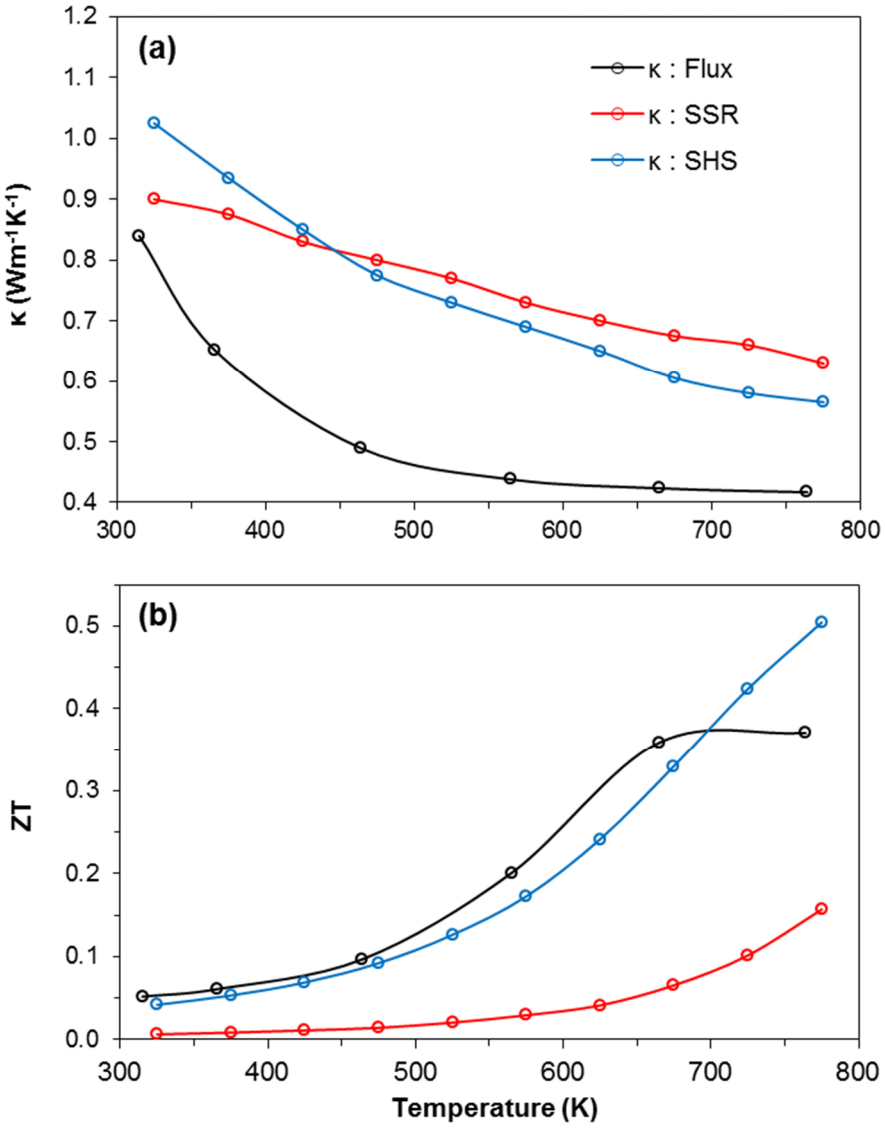

Fig. 10. Temperature dependence of SPSed BCSO synthesized by SSR, SHS and flux methods: (a) thermal conductivity; (b) thermoelectric figure of merit.

Fig. 10(b) shows temperature dependence of ZT values for the pristine BCSO synthesized using SHS-SPS, flux-SPS and SSR-SPS methods. Across a large temperature range, ZT of the materials prepared using the flux method was about the same as of the SHS method, but higher than the SSR route. As a result, BCSO showed similar ZT values (0.36 at 665 K and 0.37 at 764 K) as SHS (0.33 at 675 K and 0.49 at 775 K), but higher than that of SSR (0.09 at 675 K and 0.15 at 775K) samples [19,25,30].

3.4.2 Caesium Doped BCSO

Fig. 11 and **Fig. 12** show the temperature dependence of thermoelectric transport properties for $Bi_{1-x}Cs_xCuSeO$ (x = 0 – 0.01) samples after SPS treatment from 300 K to 680 K. As shown in **Fig. 11(a)**, the electrical conductivity of the doped samples increased with temperature. This also indicated that the monovalent Cs^+ ion was an effective dopant for BCSO. This enhancement can be explained by the increased carrier density in the TE materials. The highest electrical conductivity of ~ 25 Scm^{-1} was obtained for $Bi_{0.995}Cs_{0.005}CuSeO$ at 680 K.

The temperature dependence of Seebeck coefficient of $Bi_{1-x}Cs_xCuSeO$ is shown in **Fig. 11(b)**. At room temperature, the 1 mol% Cs doped sample exhibited a high Seebeck coefficient of ~ 550 μV/K. However, the Seebeck coefficient decreased over the whole temperature range and a similar value of ~ 370 μV/K at 680 K was observed for all samples. It is noteworthy that the trend of decreasing Seebeck coefficient with increasing temperature was observed for monovalent Cs, and an opposite effect was observed with monovalent K and Na doping [18,19]. This moderate decreased Seebeck coefficient and enhanced electrical conductivity of the doped samples produced a high-power factor value of 340 μW m^{-1} K^{-2} for $Bi_{0.995}Cs_{0.005}CuSeO$ at 680 K, as shown in **Fig. 11(c)**.

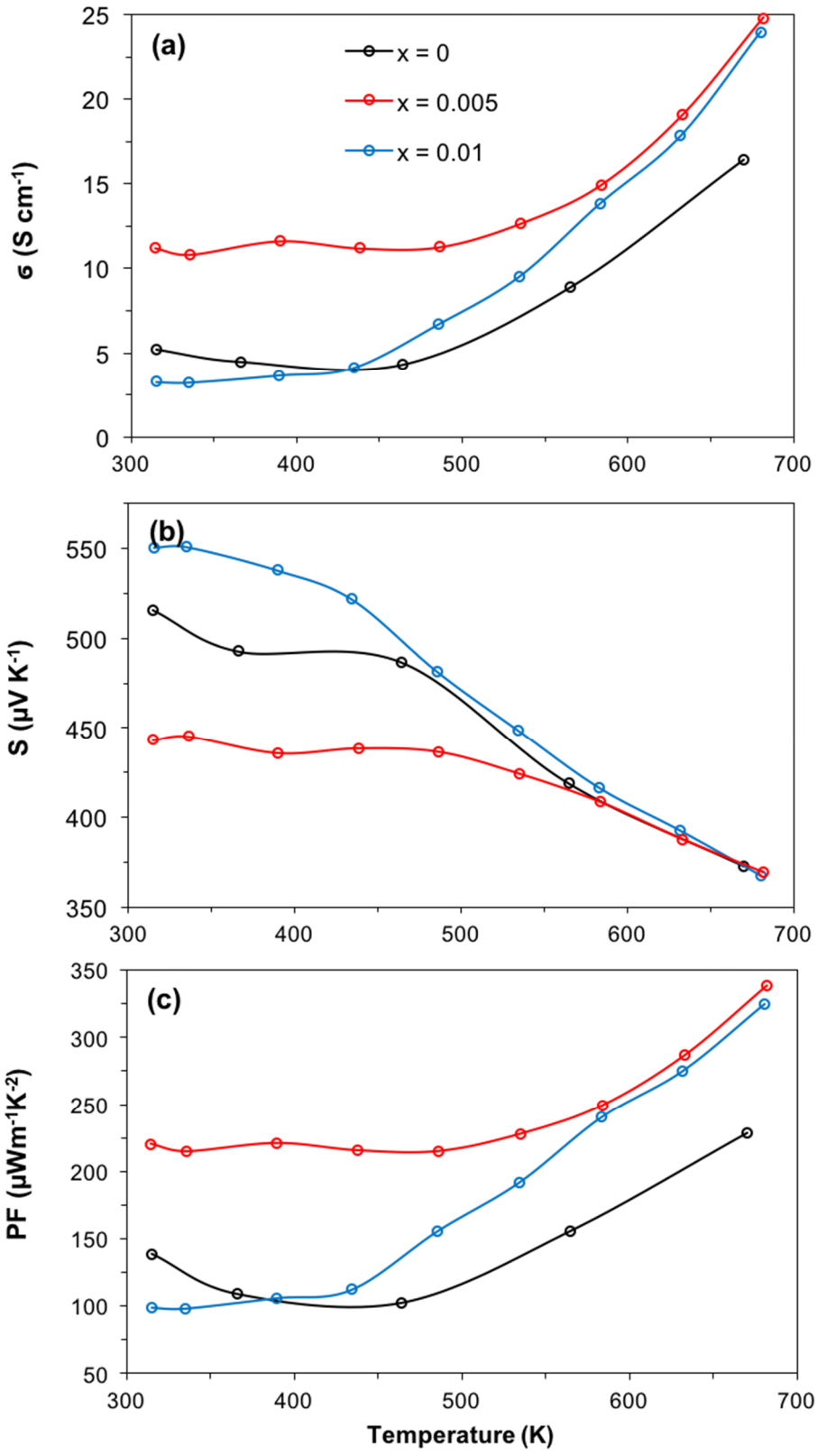

Fig. 11. Temperature dependence of SPSed $Bi_{1-x}Cs_xCuSeO$ (x = 0 – 0.01) synthesized by the flux method: (a) electrical conductivity; (b) Seebeck coefficient; (c) power factor.

Fig. 12(a) shows total thermal conductivity as a function of temperature for the $Bi_{1-x}Cs_xCuSeO$ (x = 0 - 0.01) samples. For all of the samples, the thermal conductivity decreased with rising temperature. For the undoped BCSO, a value of 0.84 $Wm^{-1}K^{-1}$ at room temperature was observed, and dropped to 0.42 $Wm^{-1}K^{-1}$ at 680 K. These values were lower than most thermoelectric materials [6,33]. Upon doping with Cs, the thermal conductivity decreased further to a minimum of 0.35 $Wm^{-1}K^{-1}$ for $Bi_{0.995}Cs_{0.005}CuSeO$ at 680K. The dimensionless figure of merit ZT is shown in **Fig. 12(b)**. ZT values increased with temperature, a maximum ZT value of 0.66 was obtained for the $Bi_{0.995}Cs_{0.005}CuSeO$ at 680 K, which was about 78 % higher than that of the pure BCSO.

The relationships between the microstructure and the electro-thermal properties of the TE materials are often complex. Generally, charge carrier density and defect density (including grain boundary density) are the most important factors. Our flux prepared prestine BCSO displayed largest grain size, highest Seebeck coefficient and lowest thermal conductivity, as compared to the SHS and SSR prepared samples. One possible explanation is that our flux prepared BCSO had an lower charge carrier density than the SHS samples at least. A lower electrical conductivity for the flux sample than for the SHS sample supports this hypothesis. This lower charge carrier density could be due to lower inpurity or defect introduced in the flux method than for the SHS method.

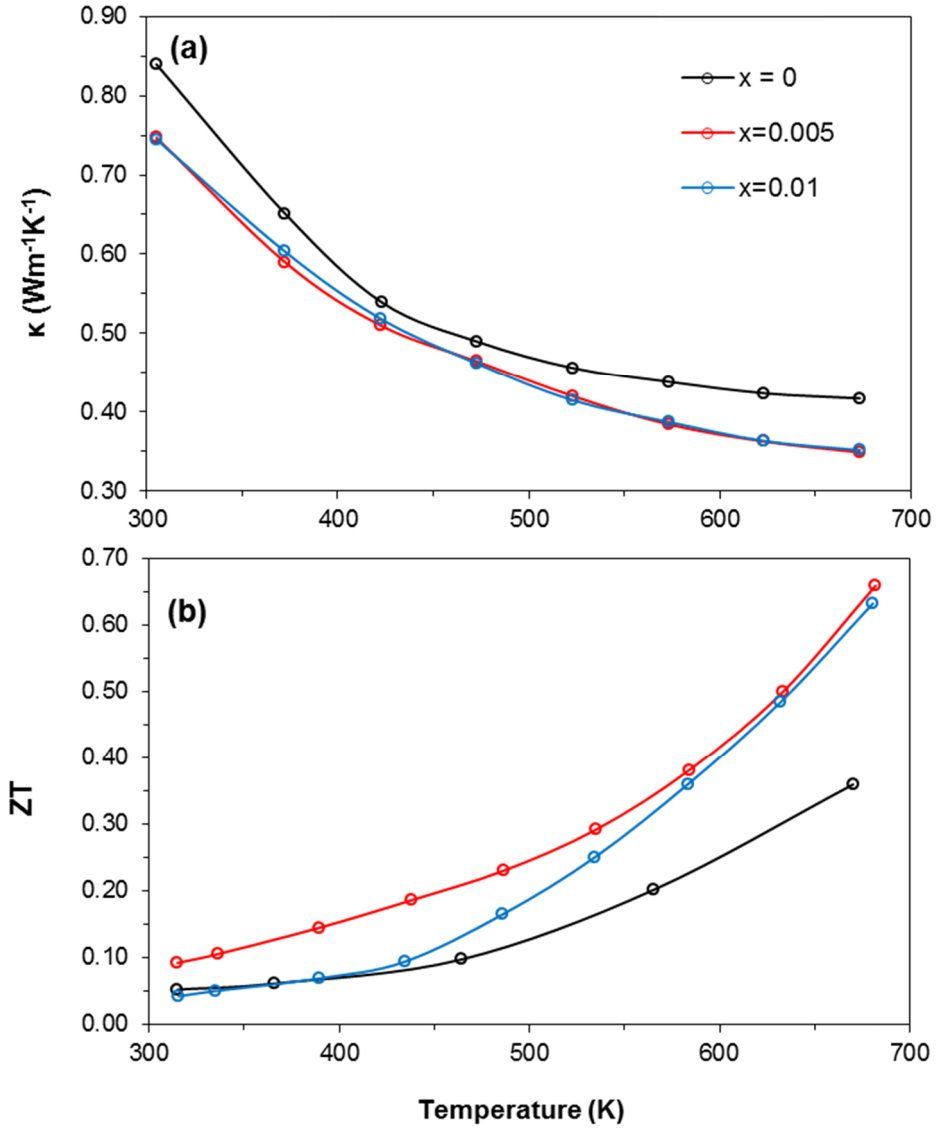

Fig. 12. Temperature dependence of $Bi_{1-x}Cs_xCuSeO$ (x = 0 – 0.01) synthesized by the flux method: (a) thermal conductivity; (b) thermoelectric figure of merit.

The incorporation of Cs on BSCO resulted in the decrease of the grain size, Seebeck coefficient, and thermal conductivity, also an increase of the electrical conductivity. One plausible explanation is that the Cs doping increased the charge carrier density. Another consequence of the incorporation of Cs into the BCSO could be the increase of point defects. This could be the reason why the 0.5% and 1% Cs doped BCSO had their thermal conductivity reduced further from that of the non-doped BCSO. Considering the hypotheis that doped BCSO had higher charge carrier density, the electrical contribution to the thermal conductivity must be much smaller than the lattice

contribution for the BCSO samples. The reduction of the grain size with doping may also contributed to the reduction of the thermal conductivity, as this increased the density of grain boundary. Furthermore, the presence of high Cs concentration areas observed for doping higher than 0,5% may be also another reason. Indeed, nanoinclusions of high Cs content can also exist and so play a role by phonon scattering in the thermal transport properties of prepared samples. Besides, the point defect scattering could also be originated from mass fluctuations and interatomic force differences between the impurity Cs (atomic mass 133) and Bi (atomic mass 209), which contribute to the lattice thermal conduction reduction, as described by Callaway [34–36]. Conclusions

The BCSO thermoelectric materials have been successfully synthesized using an eco-friendly B_2O_3 flux method. Compared with other synthesis methods, the flux method can be performed in air below 923 K with little risk of oxidation. Moreover, the BCSO prepared by the flux method had improved the electrical conductivity and Seebeck coefficient, and significantly suppressed thermal conductivity. The ZT at 680 K was increased from 0.37 for pristine BiCuSeO to 0.66 for $Bi_{0.995}Cs_{0.005}CuSeO$. These results showed promising features, such as simplicity and cost effectiveness of BCSO powder synthesis using the flux method, which may be advantageous for large-scale application.

Acknowledgments

The work was funded by a Leverhulme Trust Research Project Grant (RPG-2013-292). ZH thanks support from Hong Kong and Macao and Overseas Scholars Joint Research Fund of NSFC (No. 51428101) and Prof. P. Peng of Hunan University, China. We thank Mr. A. Stallard, T. Pryor, Drs. C. Shaw and X. Liu for technical help.

References

[1] M. Hamid Elsheikh, D.A. Shnawah, M.F.M. Sabri, S.B.M. Said, M. Haji Hassan, M.B. Ali Bashir, M. Mohamad, A review on thermoelectric renewable energy: Principle parameters that affect their performance, Renew. Sustain. Energy Rev. 30 (2014) 337–355.

[2] D. Enescu, E.O. Virjoghe, A review on thermoelectric cooling parameters and performance, Renew. Sustain. Energy Rev. 38 (2014) 903–916.

[3] X.F. Zheng, C.X. Liu, Y.Y. Yan, Q. Wang, A review of thermoelectrics research - Recent developments and potentials for sustainable and renewable energy applications, Renew. Sustain. Energy Rev. 32 (2014) 486–503.

[4] J. Yang, T. Caillat, Thermoelectric Materials for Space and Automotive Power Generation, MRS Bull. 31 (2006) 224–229.

[5] A.F. Ioffe, L.S. Stil'bans, E.K. Iordanishvili, T.S. Stavitskaya, A. Gelbtuch, G. Vineyard, Semiconductor Thermoelements and Thermoelectric Cooling, Phys. Today. 12 (1959) 42.

[6] A. Nag, V. Shubha, Oxide thermoelectric materials: A structure-property relationship, J. Electron. Mater. 43 (2014) 962–977.

[7] H. Ohta, Thermoelectric properties of $SrTiO_3$: Bulks, superlattices, and transistors, Funtai Oyobi Fummatsu Yakin/Journal Japan Soc. Powder Powder Metall. 57 (2010) 232–236.

[8] S.R. Popuri, A.J.M. Scott, R.A. Downie, M.A. Hall, E. Suard, R. Decourt, M. Pollet, J.-W.G. Bos, Glass-like thermal conductivity in $SrTiO_3$ thermoelectrics induced by A-site vacancies, RSC Adv. 4 (2014) 33720–33723.

[9] M. Molinari, D. a. Tompsett, S.C. Parker, F. Azough, R. Freer, Structural, electronic and thermoelectric behaviour of $CaMnO_3$ and $CaMnO_{(3-\delta)}$, J. Mater. Chem. A. 2 (2014) 14109.

[10] N. Wu, T.C. Holgate, N. Van Nong, N. Pryds, S. Linderoth, High temperature thermoelectric properties of $Ca_3Co_4O_9^{+\delta}$ by auto-combustion synthesis and spark plasma sintering, J. Eur. Ceram. Soc. 34 (2014) 925–931.

[11] E. Altin, E. Oz, S. Demirel, A. Bayri, Magnetic and thermoelectric properties of B-substituted $NaCoO_2$, Appl. Phys. A Mater. Sci. Process. 119 (2015) 1187–1196. doi:10.1007/s00339-015-9089-0.

[12] T. Tsubota, M. Ohtaki, K. Eguchi, H. Arai, Thermoelectric properties of Al-doped ZnO as a promising oxide material for high- temperature thermoelectric conversion, J. Mater. Chem. 7 (1997) 85–90.

[13] J.-L. Lan, Y. Liu, Y.-H. Lin, C.-W. Nan, Q. Cai, X. Yang, Enhanced thermoelectric

performance of In_2O_3-based ceramics via Nanostructuring and Point Defect Engineering, Sci. Rep. 5 (2015) 7783.

[14] J. Li, J. Sui, C. Barreteau, D. Berardan, N. Dragoe, W. Cai, Y. Pei, L. Zhao, Thermoelectric properties of Mg doped p-type BiCuSeO oxyselenides, J. Alloys Compd. 551 (2012) 649–653.

[15] C. Barreteau, D. Beardan, E. Amzallag, L. Zhao, N. Dragoe, Structural and Electronic Transport Properties in Sr-Doped BiCuSeO, Chem. Mater. 24 (2012) 3168–3178.

[16] F. Li, T.-R. Wei, F. Kang, J.-F. Li, Enhanced thermoelectric performance of Ca-doped BiCuSeO in a wide temperature range, J. Mater. Chem. A. 1 (2013) 11942–11949.

[17] J. Li, J. Sui, Y. Pei, C. Barreteau, D. Berardan, N. Dragoe, W. Cai, J. He, L.-D. Zhao, A high thermoelectric figure of merit ZT > 1 in Ba heavily doped BiCuSeO oxyselenides, Energy Environ. Sci. 5 (2012) 8543.

[18] D. Sun Lee, T.H. An, M. Jeong, H.S. Choi, Y. Soo Lim, W.S. Seo, C.H. Park, C. Park, H.H. Park, Density of state effective mass and related charge transport properties in K-doped BiCuOSe, Appl. Phys. Lett. 103 (2013) 2011–2015.

[19] J. Li, J. Sui, Y. Pei, X. Meng, D. Berardan, N. Dragoe, W. Cai, L.-D. Zhao, The roles of Na doping in BiCuSeO oxyselenides as a thermoelectric material, J. Mater. Chem. A. 2 (2014) 4903.

[20] J. Sui, J. Li, J. He, Y.-L. Pei, D. Berardan, H. Wu, N. Dragoe, W. Cai, L.-D. Zhao, Texturation boosts the thermoelectric performance of BiCuSeO oxyselenides, Energy Environ. Sci. 6 (2013) 2916.

[21] Y.-L. Pei, H. Wu, D. Wu, F. Zheng, J. He, High thermoelectric performance realized in a bicuseo system by improving carrier mobility through 3D modulation doping, J. Am. Chem. Soc. 136 (2014) 13902–13908.

[22] Y. Liu, L.-D. Zhao, Y. Zhu, Y. Liu, F. Li, M. Yu, D.-B. Liu, W. Xu, Y.-H. Lin, C.-W. Nan, Synergistically Optimizing Electrical and Thermal Transport Properties of BiCuSeO via a Dual-Doping Approach, Adv. Energy Mater. 6 (2016).

[23] L.D. Zhao, D. Berardan, Y.L. Pei, C. Byl, L. Pinsard-Gaudart, N. Dragoe, $Bi_{1-x}Sr_xCuSeO$ oxyselenides as promising thermoelectric materials, Appl. Phys. Lett. 97 (2010) 92118.

[24] F. Li, J.-F. Li, L.-D. Zhao, K. Xiang, Y. Liu, B.-P. Zhang, Y.-H. Lin, C.-W. Nan, H.-M. Zhu, Polycrystalline BiCuSeO oxide as a potential thermoelectric material, Energy Environ. Sci. 5 (2012) 7188–7195.

[25] G.-K. Ren, J.-L. Lan, S. Butt, K.J. Ventura, Y.-H. Lin, C.-W. Nan, Enhanced thermoelectric properties in Pb-doped BiCuSeO oxyselenides prepared by ultrafast synthesis, RSC Adv. 5 (2015) 69878–69885.

[26] Barreteau, D. Berardan, N. Dragoe, Studies on the thermal stability of BiCuSeO, J. Solid State Chem. 222 (2015) 53–59.

[27] F. Li, T.-R. Wei, F. Kang, J.-F. Li, Thermal stability and oxidation resistance of BiCuSeO based thermoelectric ceramics, J. Alloys Compd. 614 (2014) 394–400.

[28] C. Barreteau, D. Berardan, N. Dragoe, Studies on the thermal stability of BiCuSeO, J. Solid State Chem. 222 (2015) 53–59.

[29] G.A. Desborough, R.I. Grauch, J.G. Crock, G.P. Meeker, J.R. Herring, R.G. Tysdal., Low temperature volatilization of selenium from rock samples of the phosphoria formation on southeastern Idaho, U.S. Dept. of the Interior, U.S. Geological Survey, 2000.

[30] L.-D. Zhao, J. He, D. Berardan, Y. Lin, J.-F. Li, C. Nan, N. Dragoe, BiCuSeO oxyselenides: new promising thermoelectric materials, Energy Environ. Sci. 7 (2014) 2900–2924.

[31] Y.-L. Pei, J. He, J.-F. Li, Fuli, Q. Liu, W. Pan, C. Barreteau, D. Berardan, N. Dragoe, L.-D. Zhao, High thermoelectric performance of oxyselenides: Intrinsically low thermal conductivity of Ca-doped BiCuSeO, NPG Asia Mater. 5 (2013) e47.

[32] H. Shao, X. Tan, G.-Q. Liu, J. Jiang, H. Jiang, A first-principles study on the phonon transport in layered BiCuOSe, Sci. Rep. 6 (2016) 21035.

[33] M. Amani, I. Tougas, O.J. Gregory, Thermoelectric materials discovery using combinatorial chemistry, Mater. Res. Soc. Symp. Proc. 1315 (2012) 1–6.

[34] J. Callaway, H.C. Von Baeyer, Effect of pint iperfections on lattice thermal conductivity, Phys. Rev. 120 (1960) 1149.

[35] J. Callaway, Low-temperature lattice thermal conductivity, Phys. Rev. 122 (1961) 787.

[36] C.L. Wan, W. Pan, Q. Xu, Y.X. Qin, J.D. Wang, Z.X. Qu, M.H. Fang, Effect of point defects on the thermal transport properties of $(La_xGd_{1-x})_2Zr_2O_7$: Experiment and theoretical model, Phys. Rev. B - Condens. Matter Mater. Phys. 74 (2006).

https://dspace.org/

Enhanced thermoelectric performance of Cs doped BiCuSeO prepared through eco-friendly flux synthesis

Abdenour, Achour; Chen, Kan; Reece, Michael J.; Huang, Zhaorong

2017-11-10
Elsevier
https://doi.org/10.1016/j.jallcom.2017.11.104
Abdenour Achour, Kan Chen, Michael J. Reece, Zhaorong Huang, Enhanced thermoelectric performance of Cs doped BiCuSeO prepared through eco-friendly flux synthesis. Journal of Alloys and Compounds, Volume 735, 2018, Pages 861-869

Downloaded from a DSpace repository. https://dspace.org/